Research Article | Vol. 24, No. 24 | 28 Nov 2016 | OPTICS EXPRESS 27587

Optics EXPRESS

Improved SESAMs for femtosecond pulse generation approaching the kW average power regime

C. G. E. ALFIERI,[1,*] A. DIEBOLD,[1] F. EMAURY,[1] E. GINI,[2] C. J. SARACENO,[1] AND U. KELLER[1]

[1]*Institute for Quantum Electronics, Physics Department, ETH Zurich, 8093 Zurich, Switzerland*
[2]*FIRST Center for Micro- and Nanoscience, ETH Zürich, 8093 Zurich, Switzerland*
[*]*calfieri@phys.ethz.ch*

Abstract: We present semiconductor saturable absorber mirrors (SESAMs) that can potentially support femtosecond pulses from ultrafast thin disk lasers (TDLs) with high average power approaching the kW-power level and high pulse energy in the range of 100 µJ to 1 mJ at megahertz pulse repetition rates. For high-power operation, the SESAM parameters will ultimately limit the shortest pulse duration from a soliton mode-locked laser before mode locking instabilities such as multiple pulsing instabilities and continuous wave (cw) breakthrough start to occur. Currently shorter pulses are prevented due to the inverse saturable absorption that becomes stronger with shorter pulses and results in a shift of the "rollover" of the nonlinear SESAM reflectivity towards lower fluences. Here we discuss a novel SESAM design that addresses these issues and can be grown by metal-organic vapor phase epitaxy (MOVPE), an attractive epitaxial growth technology for manufacturing.

OCIS codes: (140.0140) Lasers and laser optics; (140.7090) Ultrafast lasers; (140.4050) Mode-locked lasers.

References and links

1. U. Keller, "Ultrafast solid-state laser oscillators: a success story for the last 20 years with no end in sight," Appl. Phys. B **100**(1), 15–28 (2010).
2. T. Südmeyer, S. V. Marchese, S. Hashimoto, C. R. E. Baer, G. Gingras, B. Witzel, and U. Keller, "Femtosecond laser oscillators for high-field science," Nat. Photonics **2**(10), 599–604 (2008).
3. U. Keller, "Recent developments in compact ultrafast lasers," Nature **424**(6950), 831–838 (2003).
4. U. Keller, K. J. Weingarten, F. X. Kärtner, D. Kopf, B. Braun, I. D. Jung, R. Fluck, C. Hönninger, N. Matuschek, and J. Aus der Au, "Semiconductor saturable absorber mirrors (SESAMs) for femtosecond to nanosecond pulse generation in solid-state lasers," IEEE J. Sel. Top. Quantum Electron. **2**(3), 435–453 (1996).
5. U. Keller, D. A. B. Miller, G. D. Boyd, T. H. Chiu, J. F. Ferguson, and M. T. Asom, "Solid-state low-loss intracavity saturable absorber for Nd:YLF lasers: an antiresonant semiconductor Fabry-Perot saturable absorber," Opt. Lett. **17**(7), 505–507 (1992).
6. J.-P. Negel, A. Loescher, A. Voss, D. Bauer, D. Sutter, A. Killi, M. A. Ahmed, and T. Graf, "Ultrafast thin-disk multipass laser amplifier delivering 1.4 kW (4.7 mJ, 1030 nm) average power converted to 820 W at 515 nm and 234 W at 343 nm," Opt. Express **23**(16), 21064–21077 (2015).
7. P. Russbueldt, T. Mans, J. Weitenberg, H. D. Hoffmann, and R. Poprawe, "Compact diode-pumped 1.1 kW Yb:YAG Innoslab femtosecond amplifier," Opt. Lett. **35**(24), 4169–4171 (2010).
8. T. Eidam, S. Hanf, E. Seise, T. V. Andersen, T. Gabler, C. Wirth, T. Schreiber, J. Limpert, and A. Tünnermann, "Femtosecond fiber CPA system emitting 830 W average output power," Opt. Lett. **35**(2), 94–96 (2010).
9. M. Müller, M. Kienel, A. Klenke, T. Gottschall, E. Shestaev, M. Plötner, J. Limpert, and A. Tünnermann, "1 kW 1 mJ eight-channel ultrafast fiber laser," Opt. Lett. **41**(15), 3439–3442 (2016).
10. C. J. Saraceno, F. Emaury, O. H. Heckl, C. R. E. Baer, M. Hoffmann, C. Schriber, M. Golling, T. Südmeyer, and U. Keller, "275 W average output power from a femtosecond thin disk oscillator operated in a vacuum environment," Opt. Express **20**(21), 23535–23541 (2012).
11. C. J. Saraceno, F. Emaury, C. Schriber, M. Hoffmann, M. Golling, T. Südmeyer, and U. Keller, "Ultrafast thin-disk laser with 80 µJ pulse energy and 242 W of average power," Opt. Lett. **39**(1), 9–12 (2014).
12. A. Diebold, F. Emaury, C. J. Saraceno, C. Schriber, M. Golling, T. Südmeyer, and U. Keller, "SESAM mode-locked Yb:CaGdAlO_4 thin disk laser with 62 fs pulse generation," Opt. Lett. **38**(19), 3842–3845 (2013).
13. C. Schriber, L. Merceron, A. Diebold, F. Emaury, M. Golling, K. Beil, C. Kränkel, C. J. Saraceno, T. S¸dmeyer, and U. Keller, "Pushing SESAM mode-locked thin-disk lasers to shortest pulse durations," in *Advanced Solid State Lasers*, OSA Technical Digest (online) (Optical Society of America, 2014), AF1A.4.

#279029 http://dx.doi.org/10.1364/OE.24.027587
Journal © 2016 Received 18 Oct 2016; accepted 9 Nov 2016; published 17 Nov 2016

Optics EXPRESS

14. C. J. Saraceno, F. Emaury, C. Schriber, A. Diebold, M. Hoffmann, M. Golling, T. Südmeyer, and U. Keller, "Toward millijoule-level high-power ultrafast thin-disk oscillators," IEEE J. Sel. Top. Quantum Electron. **21**(1), 106–123 (2015).
15. C. R. E. Baer, C. Kränkel, C. J. Saraceno, O. H. Heckl, M. Golling, R. Peters, K. Petermann, T. Südmeyer, G. Huber, and U. Keller, "Femtosecond thin-disk laser with 141 W of average power," Opt. Lett. **35**(13), 2302–2304 (2010).
16. S. Ricaud, A. Jaffres, K. Wentsch, A. Suganuma, B. Viana, P. Loiseau, B. Weichelt, M. Abdou-Ahmed, A. Voss, T. Graf, D. Rytz, C. Hönninger, E. Mottay, P. Georges, and F. Druon, "Femtosecond Yb:CaGdAlO4 thin-disk oscillator," Opt. Lett. **37**(19), 3984–3986 (2012).
17. D. E. Spence, P. N. Kean, and W. Sibbett, "60-fsec pulse generation from a self-mode-locked Ti:sapphire laser," Opt. Lett. **16**(1), 42–44 (1991).
18. J. Brons, V. Pervak, E. Fedulova, D. Bauer, D. Sutter, V. Kalashnikov, A. Apolonskiy, O. Pronin, and F. Krausz, "Energy scaling of Kerr-lens mode-locked thin-disk oscillators," Opt. Lett. **39**(22), 6442–6445 (2014).
19. J. Brons, V. Pervak, D. Bauer, D. Sutter, O. Pronin, and F. Krausz, "Powerful 100-fs-scale Kerr-lens mode-locked thin-disk oscillator," Opt. Lett. **41**(15), 3567–3570 (2016).
20. U. Keller, "Ultrafast solid-state lasers," in *Landolt-Börnstein. Laser Physics and Applications. Subvolume B: Laser Systems. Part I.*, G. Herziger, H. Weber, and R. Proprawe, eds. (Springer Verlag, Heidelberg, 2007), pp. 33–167.
21. C. J. Saraceno, C. Schriber, M. Mangold, M. Hoffmann, O. H. Heckl, C. R. E. Baer, M. Golling, T. Südmeyer, and U. Keller, "SESAMs for high-power oscillators: design guidelines and damage thresholds," IEEE J. Sel. Top. Quantum Electron. **18**(1), 29–41 (2012).
22. A. Diebold, T. Zengerle, C. G. E. Alfieri, C. Schriber, F. Emaury, M. Mangold, M. Hoffmann, C. J. Saraceno, M. Golling, D. Follman, G. D. Cole, M. Aspelmeyer, T. Südmeyer, and U. Keller, "Optimized SESAMs for kilowatt-level ultrafast lasers," Opt. Express **24**(10), 10512–10526 (2016).
23. I. D. Jung, F. X. Kärtner, L. R. Brovelli, M. Kamp, and U. Keller, "Experimental verification of soliton mode locking using only a slow saturable absorber," Opt. Lett. **20**(18), 1892–1894 (1995).
24. F. X. Kärtner, I. D. Jung, and U. Keller, "Soliton Mode-Locking with Saturable Absorbers," IEEE J. Sel. Top. Quantum Electron. **2**(3), 540–556 (1996).
25. J. Aus der Au, D. Kopf, F. Morier-Genoud, M. Moser, and U. Keller, "60-fs pulses from a diode-pumped Nd:glass laser," Opt. Lett. **22**(5), 307–309 (1997).
26. R. Grange, M. Haiml, R. Paschotta, G. J. Spuhler, L. Krainer, M. Golling, O. Ostinelli, and U. Keller, "New regime of inverse saturable absorption for self-stabilizing passively mode-locked lasers," Appl. Phys. B **80**(2), 151–158 (2005).
27. P. Langlois, M. Joschko, E. R. Thoen, E. M. Koontz, F. X. Kärtner, E. P. Ippen, and L. A. Kolodziejski, "High fluence ultrafast dynamics of semiconductor saturable absorber mirrors," Appl. Phys. Lett. **75**(24), 3841–3843 (1999).
28. C. J. Saraceno, C. Schriber, F. Emaury, O. H. Heckl, C. R. E. Baer, M. Hoffmann, K. Beil, C. Kränkel, M. Golling, T. Südmeyer, and U. Keller, "Cutting-edge high-power ultrafast thin disk oscillators," Appl. Sciences **3**(2), 355–395 (2013).
29. T. Südmeyer, C. Kränkel, C. R. E. Baer, O. H. Heckl, C. J. Saraceno, M. Golling, R. Peters, K. Petermann, G. Huber, and U. Keller, "High-power ultrafast thin disk laser oscillators and their potential for sub-100-femtosecond pulse generation," Appl. Phys. B **97**(2), 281–295 (2009).
30. C. Hönninger, R. Paschotta, F. Morier-Genoud, M. Moser, and U. Keller, "Q-switching stability limits of continuous-wave passive mode locking," J. Opt. Soc. Am. B **16**(1), 46–56 (1999).
31. L. R. Brovelli, U. Keller, and T. H. Chiu, "Design and Operation of antiresonant Fabry-Perot saturable semiconductor absorbers for mode-locked solid-state lasers," J. Opt. Soc. Am. B **12**(2), 311–322 (1995).
32. G. J. Spühler, K. J. Weingarten, R. Grange, L. Krainer, M. Haiml, V. Liverini, M. Golling, S. Schon, and U. Keller, "Semiconductor saturable absorber mirror structures with low saturation fluence," Appl. Phys. B **81**(1), 27–32 (2005).
33. M. Haiml, U. Siegner, F. Morier-Genoud, U. Keller, M. Luysberg, R. C. Lutz, P. Specht, and E. R. Weber, "Optical nonlinearity in low-temperature-grown GaAs: Microscopic limitations and optimization strategies," Appl. Phys. Lett. **74**(21), 3134–3136 (1999).
34. U. Siegner, M. Haiml, F. Morier-Genoud, R. C. Lutz, P. Specht, E. R. Weber, and U. Keller, "Femtosecond nonlinear optics of low-temperature grown semiconductors," Physica B **273–274** 733–736, (1999).
35. D. Maas, *MIXSELs - a new class of ultrafast semiconductor lasers*, Series in Quantum Electronics (Dissertation at ETH Zurich, Nr. 18121, Hartung-Gorre Verlag, Konstanz, 2009), Vol. 48.
36. D. Burns, M. Hetterich, A. I. Ferguson, E. Bente, M. D. Dawson, J. I. Davies, and S. W. Bland, "High-average-power (>20 W) Nd:YVO_4 lasers mode locked by strain-compensated saturable Bragg reflectors," J. Opt. Soc. Am. B **17**(6), 919–926 (2000).
37. N. Xiang, H. F. Liu, J. Kong, D. Y. Tang, and M. Pessa, "Monolithic semiconductor saturable absorber mirror with strain-compensated GaInAs/GaAsP quantum wells," J. Cryst. Growth **301–302** 989–992, (2007).
38. U. Keller and A. C. Tropper, "Passively mode-locked surface-emitting semiconductor lasers," Phys. Rep. **429**(2), 67–120 (2006).
39. J. W. Matthews and A. E. Blakeslee, "Defects in epitaxial multilayers," J. Cryst. Growth **27**, 118–125 (1974).

Optics EXPRESS

40. E. W. Van Stryland, M. A. Woodall, H. Vanherzeele, and M. J. Soileau, "Energy band-gap dependence of two-photon absorption," Opt. Lett. **10**(10), 490–492 (1985).
41. M. Haiml, U. Siegner, F. Morier-Genoud, U. Keller, M. Luysberg, P. Specht, and E. R. Weber, "Femtosecond response times and high optical nonlinearity in beryllium-doped low-temperature grown GaAs," Appl. Phys. Lett. **74**(9), 1269 (1999).
42. M. Mangold, V. J. Wittwer, C. A. Zaugg, S. M. Link, M. Golling, B. W. Tilma, and U. Keller, "Femtosecond pulses from a modelocked integrated external-cavity surface emitting laser (MIXSEL)," Opt. Express **21**(21), 24904–24911 (2013).
43. D. J. H. C. Maas, B. Rudin, A.-R. Bellancourt, D. Iwaniuk, S. V. Marchese, T. Südmeyer, and U. Keller, "High precision optical characterization of semiconductor saturable absorber mirrors," Opt. Express **16**(10), 7571–7579 (2008).

1. Introduction

Ultrafast solid-state lasers have a tremendous impact in many disciplines of science and technology [1–3]. Stable passive mode locking of diode-pumped solid-state lasers became possible using the semiconductor saturable absorber mirror (SESAM) [4,5]. Today diode-pumped solid-state laser amplifier systems seeded by SESAM mode-locked laser oscillators achieved average output powers above 1 kW. This was made possible with improvements in laser diode arrays together with the development of power-scalable laser configurations with optimized heat removal geometries based on the thin disk (generating 1.4 kW average power, 4.7 mJ, 8 ps pulses at 300 kHz [6]), the Innoslab (generating 1.1 kW, 5.5 µJ, 615 fs at 200 MHz [7]), and the fiber amplifier systems (generating 830 W, 11 µJ, 640 fs at 78 MHz from a single fiber amplifier or 1 kW, 1 mJ, 260 fs at 1 MHz from the coherent combination of several fiber amplifiers [8,9]). The complexity, reliability, noise and pulse quality can potentially be improved when these multi-stage amplifier systems can start with a high-power ultrafast laser oscillator.

The current state-of-the-art for high-power/high-energy ultrafast laser oscillators is based on SESAM mode-locked Yb:YAG thin disk lasers (TDLs) generating either a record high average power of 275 W with 16.9 µJ, 583 fs pulse durations at 16.3 MHz pulse repetition rate [10] or a record high pulse energy of 80 µJ at 242 W average output power, 1 ps pulse durations at 3 MHz [11]. Pulses shorter than 50 femtoseconds can be achieved with novel gain materials [12,13], but at the expense of much lower average power and pulse energy. We have explored many different laser materials to obtain shorter pulse durations while keeping the multi-100-W average power [14], with the most promising gain materials being Yb:LuO [15] and Yb:CALGO [16]. Alternatively Kerr-Lens mode locking (KLM) [17] provides a faster saturable absorber and has led to shorter pulse durations at somewhat lower output power [18,19]. This, however, comes with the well-known trade-off of no self-starting of the mode locking process and a nonlinear coupling of the saturable absorber action to the laser cavity stability which requires very critical cavity mirror position adjustments [20]. Much further average power scaling with KLM TDLs will become more challenging due to thermal effects. Therefore, overcoming the existing trade-off between pulse duration and average power with SESAM mode-locked TDLs remains an important challenge to solve.

In high-power ultrafast TDLs all cavity elements need to withstand very high fluences, and SESAMs should not run into the rollover or damage regime, nor introduce excessive thermal lensing. Previously we have understood and solved the damage problem for SESAMs [21] and improved the flatness and thermal lens of SESAMs with a novel heatsink technology [22], which continues to support further power-scaling by increasing the cavity mode size on the SESAM in analogy to the thin disk gain crystal. Here in this paper we address the SESAM limitations for shorter pulse generation with soliton mode locking [23,24], while keeping the average power in the multi-100-W to kW regime. In the femtosecond regime, the inverse saturable absorption is dominated by two photon absorption (TPA), thus stable soliton mode locking can only be obtained with longer pulses with the current SESAM parameters. We can demonstrate here that we can adjust the SESAM parameters for shorter pulse operation with strain-compensated fast SESAMs with a higher damage threshold and a higher rollover

Optics EXPRESS

fluence. With such SESAMs we not only should be able to support shorter pulse generation, but we also obtain a higher damage threshold and lower thermal lensing when mounted on a better heatsink. Furthermore, we demonstrate here that such improved SESAMs can be grown by metal-organic vapour phase epitaxy (MOVPE), an attractive epitaxial growth technology for manufacturing.

The paper is organized as follows. In section 2 we briefly define all relevant SESAM parameters and explain the challenge of adjusting these parameters for both shorter pulse generation and high average power/high pulse energy. In section 3 we introduce the different SESAM structures under test. In section 4 we present the linear and nonlinear SESAM characterization with the successfully demonstrated improved SESAM parameters. We then summarize all our results in the final section.

2. SESAM parameters for shorter high-power pulse durations

2.1 Definition of SESAM parameters

In the following we present the targeted SESAM parameters and the trade-offs that need to be overcome. A typical fluence-dependent SESAM reflectivity is shown in Fig. 1. For mode locking of TDLs in high-power, short-pulse regime, a large saturation fluence F_{sat} (hundreds of μJ/cm^2) is typically preferred, to operate with reasonably small laser spot sizes in less sensitive resonator designs. In addition, a moderate modulation depth ΔR of around 1% is typically used as the gain per roundtrip is low for TDLs using only one single gain path per roundtrip. Moderate to short recovery time $\tau_{1/e}$ (< 20 ps) is desired to reach shorter pulses. The non-saturable loss ΔR_{ns} should be kept as small as possible for minimal thermal effects. The reflectivity "rollover" is defined by the fluence F_0, for which the saturated reflectivity is reaching its maximum value. Shifting the rollover to high fluences is required to avoid multiple pulsing instabilities and damage [21,25].

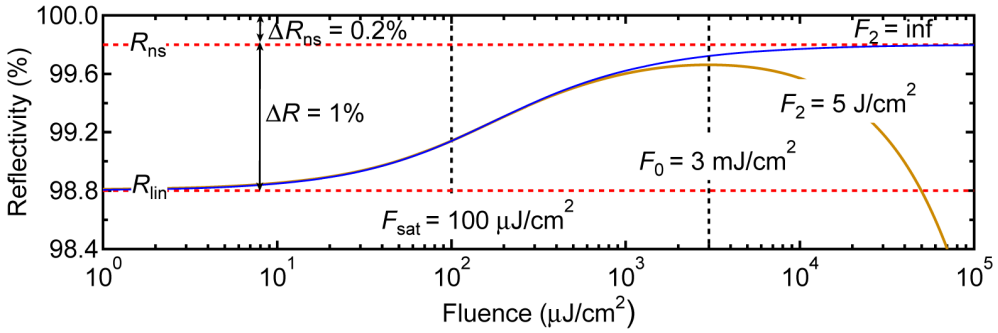

Fig. 1. Definition of SESAM parameters: Example of a typical nonlinear reflectivity curve of a high-power SESAM, showing all relevant saturation parameters. The quantity F_0 represents the fluence at which the reflectivity reaches its maximum. In case of infinite F_2, no rollover can be observed and F_0 is infinite as well.

In order to characterize the strength of the reflectivity rollover, we use the parameter F_2, which describes the inverse saturable absorption observed in the high-fluence regime [26]. In the femtosecond domain, the inverse saturable absorption is dominated by TPA. Thus with the assumption of sech^2 pulse shape typically observed for soliton mode locking, F_2 is determined by [27]:

$$F_2 = \frac{\tau_p}{0.585 \int \beta_{TPA}(z) n^2(z) |E(z)|^4 \, dz} \tag{1}$$

with z being the vertical position in the epitaxial layer stack, $E(z)$ the normalized electric field in the structure, $n(z)$ the refractive index, $\beta_{TPA}(z)$ the material-dependent TPA coefficient

Optics EXPRESS

and τ_p the duration of the incident pulse. According to this formula, shorter pulses lead to a decreased F_2 coefficient at a given pulse fluence and subsequently to an earlier rollover effect of the SESAM. Therefore, this is a critical design parameter for shorter pulse generation.

2.2. Optimized SESAM parameters for shorter high-power pulse generation

We have demonstrated that, as long as the SESAMs are not operated deep in the reflectivity rollover, thermal effects do not affect the TDL performance and we can benefit from the thin SESAM structure (i.e. typically a few micrometers thick) in combination with large laser spot sizes (i.e. around a few centimeters) to obtain a quasi-one-dimensional heat flow similar to the thin disk geometry in the gain medium. In this regime, power scaling is possible by simply increasing the laser cavity mode size on the SESAM, which keeps a constant saturation level.

To date, all our high-power SESAMs were designed and fabricated for mode locking with pulse durations in the order of 1 ps, i.e. SESAMs with moderate modulation depth in the order of 1% or less, saturation fluences of ≈100 μJ/cm^2 and recovery times of several tens to hundreds of picoseconds.

The SESAMs that will support significantly shorter pulses (i.e. < 300 fs) at high average power will require a more demanding set of parameters. In particular, high average power operation needs SESAMs with higher saturation fluence, high-damage threshold, a rollover shifted towards higher fluence, and lower non-saturable losses. However, there is a trade-off. Shorter pulses need fast recovery times (i.e. a few picoseconds) [28,29], low TPA and a large ΔR (>1%) limited by the onset of Q-switching instabilities [30] or multiple pulsing instabilities [20,25]. These SESAM parameters become challenging to be achieved simultaneously because the combination of higher rollover, increased modulation depth and faster recovery times in antiresonant SESAM designs [31,32] requires a top reflector with larger reflectivity and an increased number of absorber layers. For fast recovery we use quantum well (QW) absorber layers grown at lower temperature to increase mid-gap defects [33], which are difficult to obtain with a low level of non-saturable loss and a good crystalline quality [34]. The higher number of absorber quantum wells at an operation wavelength around 1 μm requires InGaAs quantum wells which needs strain compensation because of the lattice mismatch of InGaAs QWs and AlGaAs/GaAs Bragg mirrors.

2.3. Antiresonant SESAM with higher reflectivity of dielectric top coatings

An antiresonant SESAM [31,32] with a high reflectivity of the dielectric top coating gives a high saturation fluence and a high rollover. An increase of the F_2 parameter can be achieved by minimizing the electric field in the antiresonant SESAM where materials with strong TPA are present (Fig. 2). Thus with the dielectric top coatings we will limit the high field strength to the dielectric material which has a much lower TPA than the semiconductor material [21]. However, there is a trade-off with regards to the modulation depth:

- Large F_{sat}: for a given antiresonant SESAM structure the product of saturation fluence and modulation depth (F_{sat}•ΔR) is a fixed intrinsic quantity, not adjustable by changing the reflectivity of the top coating [21, 35]. Thus a higher reflectivity of the top coating will result in a higher F_{sat} [31], but also will reduce ΔR eventually so much that no stable soliton mode locking can be achieved.
- Large ΔR*:* with an increased number of QWs we can increase the overall product F_{sat}•ΔR. However, for an operation wavelength of around 1 μm we need InGaAs QWs which are not lattice matched on GaAs. Thus different material layers are then required to balance the tensile stress induced by the lattice mismatch between the InGaAs QWs and the GaAs substrate [36, 37]. For 1030 nm, we use InGaAs QWs with 25% of In.

Optics EXPRESS

So far, high-power SESAMs have only been demonstrated with a low number of QWs (up to 4). As we need to increase the top coating we also need to increase in the product F_{sat}•ΔR and therefore need to increase the number of quantum wells and add strain-compensation.

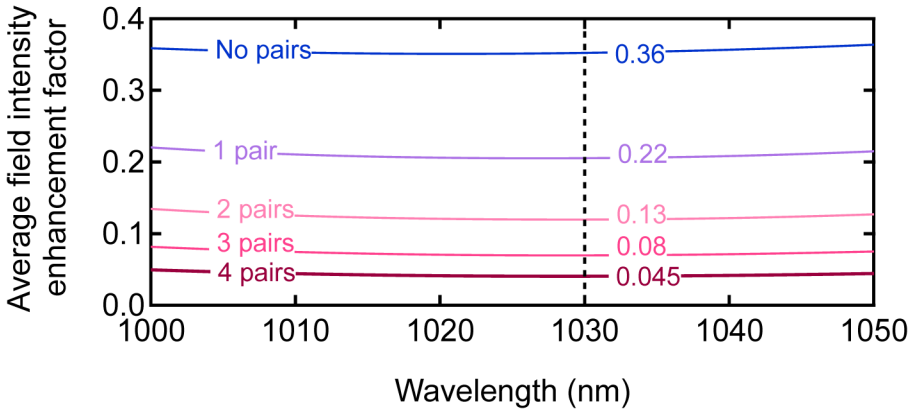

Fig. 2. Average field intensity enhancement factor (normalized to 4 outside of a 100% mirror) [32] at the quantum well (QW) position of an antiresonant SESAM for different numbers of SiO_2/Si_3N_4 λ/4 layer pairs in the delectric top coating. Adjusting the top coating modifies ΔR and F_{sat}, while keeping the product F_{sat}•ΔR constant. The flat spectral profile is beneficial for short pulse generation. Numerical inset values refer to the center wavelength of 1030 nm (vertical dashed line).

2.4 Strain compensation with lower TPA

We will discuss below the first generation of strain-compensated, high-power SESAMs grown by metal-organic vapour phase epitaxy (MOVPE) with fast recovery dynamics and low TPA. Traditionally, passive and active strain-compensated multi-QW semiconductor structures for operation around 1030 nm use low-bandgap GaAsP materials (e.g. a bandgap $E_g \approx 1.5$ eV for $GaAs_{93}P_7$) to balance the strain and maintain a high crystal quality (Fig. 3.(a)) [36–39]. However, the TPA coefficient β_{TPA} is comparatively high for low-bandgap semiconductors [40] and the insertion of thick GaAsP layers in a multi-QW high-power SESAM would eventually cause a low-fluence reflectivity rollover and lower damage threshold.

Therefore, for strain-compensated SESAMs with reduced TPA, we developed large-bandgap quaternary AlGaAsP materials (e.g. $E_g > 2.2$ eV for $Al_{98}Ga_2As_{100-x}P_x$) with low β_{TPA} (Fig. 3(b)). These materials are implemented for the first time to our knowledge in a SESAM structure. Strain compensation provided by large-bandgap AlGaAsP materials with negligible TPA coefficients allows us to significantly increase the number of QWs from the typical value of 3 (as in [10,11]) to 8 without increasing the nonsaturable losses. In accordance to our guidelines, this increase in the number of absorber layers together with the higher reflectivity of the dielectric top coating gives a higher F_{sat}, a higher reflectivity rollover, and a higher damage threshold. In addition the excellent crystal quality of the this SESAM results in a higher heat conductivity and makes them suitable for post-processing with better heat sinks as described in more details in [22].

Our best SESAM discussed in the next section has an F_{sat} of 334 μJ/cm^2, a ΔR of 1.3%, a fast recovery time (1/e) of 17 ps, extremely low non-saturable loss of 0.14% and a damage threshold higher than 100 mJ/cm^2. In combination with our novel bonding techniques [22], these SESAMs will be a key-enabling component for the next power and energy scaling of ultrafast oscillators with shorter pulse durations.

Optics EXPRESS

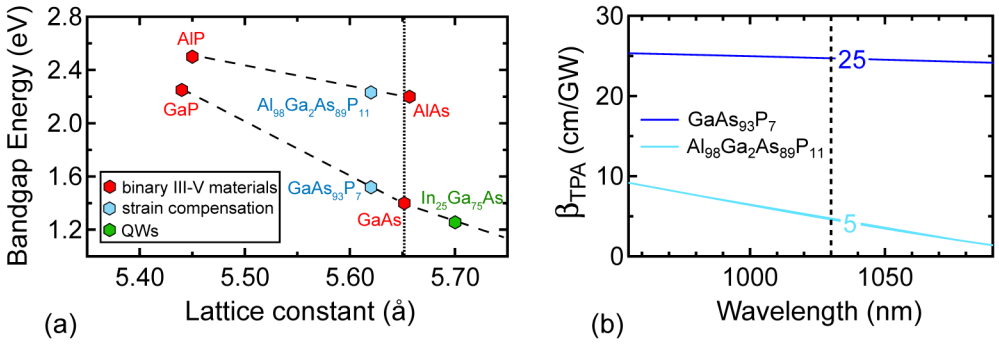

Fig. 3. (a) Bandgap energy E_g and crystal lattice constant of our semiconductor materials of interest. Dotted vertical line: perfect matching to the lattice constant of the GaAs substrate. In light blue, compounds which can be used to compensate the tensile strain introduced by the InGaAs QWs (green). (b) TPA coefficient for low-bandgap GaAsP and large-bandgap AlGaAsP strain compensation materials calculated as in [40]. Low values for β_{TPA} are preferred to reduce the rollover fluence. The numerical inset values refer to a center wavelength of 1030 nm (dashed line).

2.5 Fast SESAMs with low nonsaturable losses

Normally we observe a trade-off between fast recovery time of the saturable absorption and the nonsaturable losses:

- Short $\tau_{1/e}$: low-temperature growth of QW absorber layers is typically used to introduce mid-gap defects in form of As antisites. The positively charged antisites act as very efficient electron traps and therefore reduce the absorber recovery time [41].
- Low ΔR_{ns}: The short recovery time comes at the expense of higher non-saturable losses. The mid-gap electron traps are the positively charged As antisites but low-temperature epitaxial growth introduces a much higher density of neutral antisites which have a strong absorption cross section into the conduction band. This increases the nonsaturable losses because these highly excited electrons will not saturate this absorption and will relax via electron-phonon interactions to the bottom of the conduction band which is energy transferred into heat. These nonsaturable loss can be reduced through annealing which forms As precipitates that still form good electron traps but have no strong transition cross section for absorption into the conduction band. But again there is a trade-off because this annealing tends to make the saturable absorbers slower, ultimately requiring a compromise [33, 34, 38]. We recently discovered that low-temperature grown InGaAs QW embedded in AlAs barriers can generate electron traps with even faster recombination which also remain fast with longer annealing times [42].

3. SESAMs under test

We compare four SESAM structures (Fig. 4) grown in the FIRST cleanroom facility at ETH Zurich. All structures used in this study were grown on 100-oriented GaAs substrates both by MBE (*Veeco Instruments Inc., St. Paul, MN, United States*) and MOVPE (AIX 200/4 *AIXTRON SE, Herzogenrath, Germany*). We carried out all growth for the strain-compensated SESAMs on our MOVPE machine.

MBE-grown SESAM (MBE: 1x3 SQW): This SESAM is used as a reference sample, as it is the SESAM we used for the prior record TDL results [10, 11]. The structure of this SESAM (Fig. 4(a)) consists of a high-temperature grown (580°C) 30-pair AlAs/GaAs distributed Bragg reflector (DBR) with high-reflectivity bandwidth centered at 1030 nm. The absorber section consists of three strained quantum wells (SQWs), each with a InGaAs thickness of 10 nm embedded in AlAs barriers and placed in one single antinode of the

Optics EXPRESS

electric field standing wave pattern. No strain compensation is included and the absorber layers were grown at moderately low temperature (280°C) to carefully balance the trade-off between low ΔR_{ns} and fast recovery time. On top of a GaAs cap layer optimized to make the structure fully antiresonant, we added a 3-pair SiO_2/Si_3N_4 dielectric top mirror deposited through plasma-enhanced chemical vapor deposition (PECVD). We will refer to this device as the 1x3 SQW SESAM. Without strain compensation, larger number of QWs was not possible without strong degradation of the crystal and surface quality.

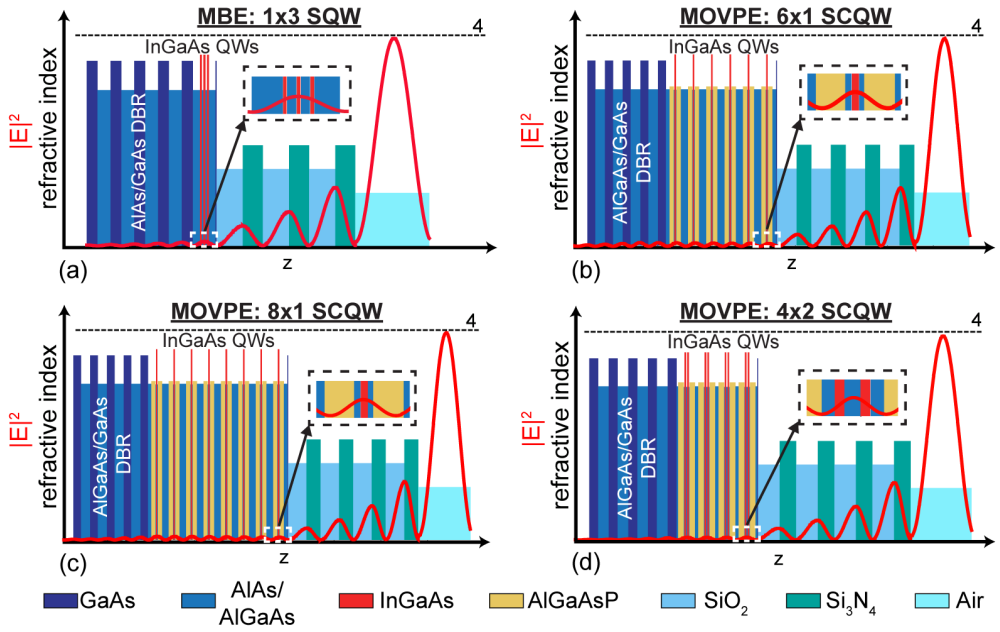

Fig. 4. Overview of the SESAM structures under test. (a) 3 strained QW SESAM with a top coating of 3 pairs of SiO_2/Si_3N_4 layers. (b) 6 strain compensated QWs, one per antinode with a 4-pair top coating. (c) 8 strained compensated QWs, one per antinode with a 4-pair top coating. (d) 8 strained compensated QWs, 2 per antinode with 4-pair top coating.

MOVPE-grown SESAMs: the lower high reflector inside the SESAM structure is obtained with a 27-pair $Al_{98}Ga_2As$/GaAs DBR (reflectivity > 99.99%) grown at 750°C, followed by an additional saturable absorber section. The final dielectric top coating is the same for all these SESAMs:

- 6 strain-compensated QWs (SCQWs), each 13-nm thick and grown at the relatively low temperature (for MOVPE) of 570°C, one per antinode of the electric standing wave pattern. They are surrounded by 5-nm thick AlAs barriers and strain compensation is provided by $Al_{98}Ga_2As_{89}P_{11}$ layers grown at 660°C. We refer to this SESAM design as the 6x1 SCQW (Fig. 4(b)).
- 8 SCQWs, each 13-nm thick, one per antinode, surrounded by AlAs barriers and grown at 570°C as for the 6x1 SCQWs. $Al_{98}Ga_2As_{89}P_{11}$ (660°C) was used for compensation (Fig. 4(c)). We will refer to this SESAM design as the 8x1 SCQW.
- 8 SCQWs, 13-nm thick, placed in pairs symmetrically around one antinode of the standing electric field. The QWs and the thin AlAs barriers were again grown at 570°C. A strain-compensating layer of $Al_{98}Ga_2As_{84}P_{16}$ (660°C) was used here because of the limited space between two successive antinodes: the higher P content (i.e. a greater compressively strain) provides compensation for the higher strain of two QWs (Fig. 4(d)). This more compact solution comes at the expense of a higher

Optics EXPRESS

sensitivity to growth errors: a small error on the actual AlGaAsP thickness can result in an over/under compensated SESAM. We will refer to this SESAM design as the 4x2 SCQW.

A GaAs cap layer is optimized for antiresonance and forms the final semiconductor layer of each structure. The designed field intensity enhancement factor in the QWs before top coating is comparable for all the MBE and MOVPE samples. A 4-pair dielectric DBR (SiO_2/Si_3N_4) was deposited on top of each MOVPE structure for strong field intensity reduction to maximize F_{sat}, while still achieving a moderate ΔR of >1%. These parameters are ideal for pushing output powers to the kilowatt level. As described above, however, by adapting the top coatings we can easily shift the values of ΔR and F_{sat}. Future lasers primarily intended for even shorter femtosecond pulses might need higher ΔR (in the order of 3%) and lower F_{sat}, which can readily be achieved by adjusting the top coating.

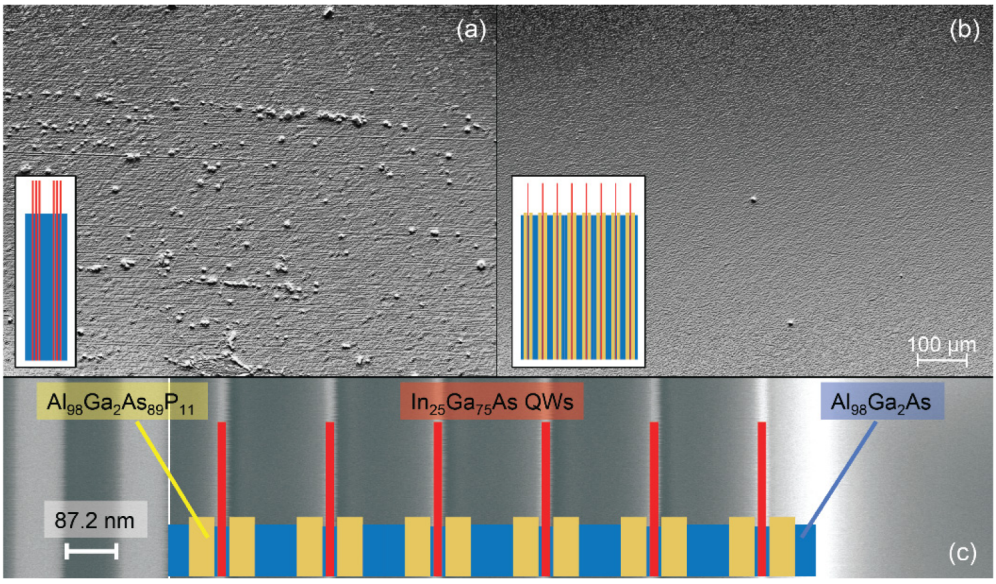

Fig. 5. Microscopic SESAM surface comparison using a Normaski phase contrast microscope: (a) 3x2 strained QW MBE SESAM (not described in the main text): strain lines, as well as a high defect density are visible. (b) 8x1 SCQW sample: strain compensation significantly reduces the defect density; no strain lines are visible even with an increased number of QWs. (c) SEM picture of the 6x1 SCQW absorber section showing a perfect overlap with the design structure.

The benefits of strain compensation can be recognized through microscopic investigation of the semiconductor surface. Figure 5(a) shows how a non-compensated 6-QW absorber section (not previously described) leads to a high defect density, making the sample inappropriate for our low-loss resonators and for our delicate substrate removal and bonding techniques [22]. In contrast, thanks to the careful calibration of the P content and thickness of the AlGaAsP layers, we obtained an almost defect-free surface for the 8x1 SCQW (Fig. 4(b)). The growth accuracy is verified through scanning electron microscopy (SEM): in Fig. 4(c) one can observe the close correspondence between design and actual grown absorber section for the 6x1 SCQW.

4. Nonlinear reflectivity and damage measurements

4.1 Nonlinear reflectivity

We measured the nonlinear reflectivity of our SESAMs in the high-precision reflectivity characterization setup described in [43]. To probe the samples with high fluence, (comparable

Optics EXPRESS

to those achieved inside our mode-locked thin-disk oscillators), we used a SESAM mode-locked Yb-YAG thin-disk laser emitting 1-ps pulses at 1030 nm with an average output power of 5 W at 3.9 MHz of pulse repetition rate (pulse energy ≈1.3 µJ). With a focused 10 µm spot size on the sample we could reach a maximum incident fluence on the devices > 0.2 J/cm^2. Through an attenuation stage, we measured the reflectivity of the devices under test varying the fluence over an unprecedented large fluence range of 5 orders of magnitude. The experimental data points, numerically taking into account the Gaussian beam shape, were then fitted through least-squares methods to the same reflectivity model used in [21] in order to extract the relevant saturation parameters presented in Fig. 1.

Figure 6(a) shows the saturation curves we obtained for the different analyzed SESAMs and Table 1 reports numerical values for the fitted parameters.

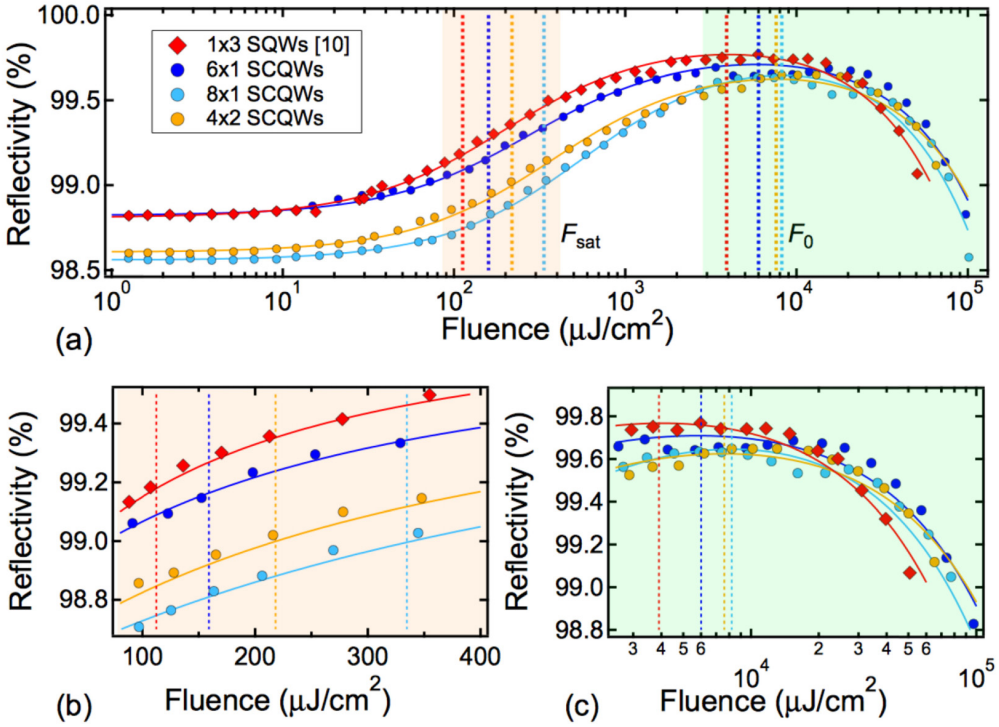

Fig. 6. (a) Nonlinear reflectivity measurements of the SESAMs under test. Dots: measured points; solid line: least square fit. (b) On a linear scale, zoom into the fluence range containing F_{sat}. (c) On a log-scale, zoom into the high-fluence regime containing F_0.

The modulation depth for all SESAMs is between 1% and 1.3% which have been typical values for ultrafast TDLs with one or two single gain path per cavity roundtrip [10,11]. On the other hand, the strain compensated SESAMs have a higher saturation fluence, i.e. 45% to 170% higher compared to the 120 µJ/cm^2 of the 1x3 SQW SESAM (Fig. 6(b)). This is achieved with the combination of the larger number of QWs (which increased the intrinsic product F_{sat}•ΔR) and the dielectric top coating with a higher reflectivity. The strongly reduced field intensity keeps the modulation depth at moderate values and increases the saturation fluence. In addition, we obtained an F_2 parameter at least 50% higher compared to the 1x3 SQW.

The thicker absorber in principle have a thicker material section with a higher potential for TPA. However, the low-β_{TPA} high-bandgap materials in combination with the weaker field intensity keeps the nonsaturable losses low. Despite the large number of QWs and the relatively low growth temperature, we observe only a small increase of ΔR_{ns} for the MOVPE

Optics EXPRESS

SESAMs (Table 1). Our strain compensation therefore balanced additional losses, usually coming from a degraded crystal quality.

The rollover is generally shifted to higher fluence. In particular, the 8x1 SCQWs SESAM has an F_0 parameter more than doubled compared to the 1x3 SQW SESAM. In a high-power oscillator, this would mean that twice the intra-cavity pulse energy can be reached without damage and multiple pulsing instabilities. In Fig. 6(c) we observe how in the high-fluence range starting from 20 mJ/cm^2 (where the next generation of high-power TDLs will probably operate) the novel samples show significantly weaker rollover compared to the 1x3 SQW SESAM.

4.2 Damage threshold

We performed damage tests on our different SESAM structures. We consider a SESAM damaged at a certain fluence when we observe a rapid irreversible drop in reflectivity (>50%). Thus we measure and define a damage fluence threshold (F_d) as described in Ref [21]. before. To extract the SESAM F_d parameters (Table 1), we used the nonlinear reflectivity measurement setup to scan the incident fluence with small steps of ≈1.5 mJ/cm^2, starting well within the rollover regime.

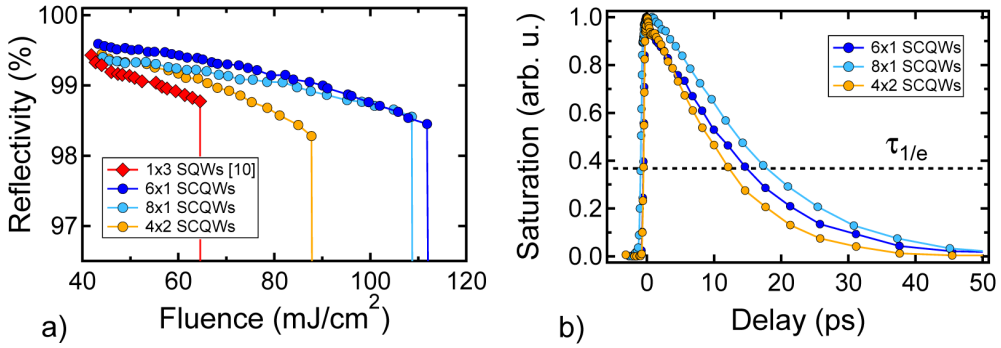

Fig. 7. (a) Nonlinear reflectivity measurements with fine high-fluence scans to precisely determine the damage fluence. (b) Pump-probe measurements revealing fast saturation recovery times for the strain compensated samples.

The strain-compensated SESAMs show significantly higher damage fluence in all cases compared to the 1x3 SQW. In particular, the 1x6 and 1x8 SCQWs have F_d exceeding 100 mJ/cm^2. The more critical sensitivity to growth errors could have led to non-perfect compensation for the 4x2 SCQWs, therefore introducing more defects and finally a slightly lower F_d. Nevertheless, for all these SESAMs, damage occurs in a regime where no SESAM mode-locked laser could operate stably (Fig. 7(a)). It is important to notice that a higher ΔR can be obtained in a straightforward way: simply by applying less top coating pairs. For example, the nonlinear reflectivity measurements on the 6x1 SCQWs SESAM coated with just one dielectric pair in the top coating showed a $\Delta R > 3\%$, combined with F_{sat} ≈50 µJ/cm^2 and still high damage threshold of 31 mJ/cm^2.

5. Recovery time

We also measured the recovery dynamics of the MOVPE SESAMs under test. The recovery time ($\tau_{1/e}$) is defined by the time delay when the reflectivity is recovered to the 1/e – value of its maximum saturation. We used a standard degenerate pump-probe setup with a Ti:sapphire laser delivering 800 mW of average output power in 130-fs pulses at a center wavelength of 1030 nm and 80 MHz of pulse-repetition rate (≈10 nJ of pulse energy). The samples were pumped at a fluence of approximately F_{sat} and probed with weak fluence of less than 2µJ/cm^2.

Optics EXPRESS

As one can see in Table 1 and Fig. 7(b), we extracted a fast recovery for the MOVPE samples of 12-17 ps. The thinner absorber region supported even faster recovery times but at the expense of a somewhat lower damage threshold.

Since two different epitaxial machines were used, a direct MBE-MOVPE growth temperature comparison is not possible. We assume that an epitaxial growth temperature of 570°C in the MOVPE introduced an amount of defects sufficient to support a fast response. The nonsaturable losses of the strain-compensated SESAMs, however, stayed low despite the fast recovery times. The high crystal quality preserved by the strain compensation, together with the higher finesse of the antiresonant Fabry-Perot, balanced the effect of low-temperature growth and kept the losses < 0.2%. We therefore achieved fast recovery times in combination with low nonsaturable losses with our MOVPE SESAMs, which is required for further power scaling of ultrafast solid-state lasers.

Table 1. Measured nonlinear parameters, damage threshold and recovery time

SESAM	F_{sat} (μJ/cm^2)	ΔR (%)	ΔR_{ns} (%)	F_2 (J/cm^2)	F_0 (mJ/cm^2)	F_d (mJ/cm^2)	$\tau_{1/e}$ (ps)
1x3 SQW	120	1.1	0.10	6.0	3.9	64	67 [10]
6x1 SCQW	174	1.0	0.14	10	5.8	112	15
8x1 SCQW	334	1.3	0.14	9.0	8.2	108	17
4x2 SCQW	246	1.2	0.18	9.2	7.0	88	12

1x3 SQW: 3 strained QWs in one single antinode. 6x1 SCQW: 6 strain-compensated QWs, one per antinode. 8x1 SCQW: 8 strain-compensated QWs, one per antinode. 4x2 SCQW: 8 strain-compensated QWs, 2 per antinode. The errors for the values here presented are below 15%.

6. Conclusion and outlook

We presented the first generation, to the best of our knowledge, of multiple-QW SESAMs strain-compensated with large bandgap materials. Our SESAMs were specifically designed for high-power, ultrafast thin-disk lasers, but the designs presented here can be extended to other types of high-power oscillators. Our fabrication guidelines are based on a higher number of QWs (6 or 8 in this case) with a higher reflectivity of the dielectric top coating. Our SESAMs combine fast recovery times in the 10-ps range, with high saturation fluence, moderate to high modulation depth, extremely low nonsaturable loss (i.e. $\Delta R_{ns} << \Delta R$) and high damage threshold. Excellent epitaxial quality required for post processing and bonding on better heatsinks [22] and large defect-free area, were achieved with excellent strain compensation, which balances the large structural stress induced by lattice mismatch between the GaAs substrate and the InGaAs QWs at an operation wavelength of 1030 nm. To avoid the negative impact of thick strain compensation layers on the inverse saturable absorption parameters, we optimized large-bandgap AlGaAsP compounds with low TPA coefficients.

We compared the saturation and damage parameters of our novel SESAMs to that of previous state-of-the-art MBE SESAM that enabled the record-high results in output power and pulse energy [10,11]. All our novel SESAMs have higher saturation fluences (up to > 300 μJ/cm^2) with comparable modulation depths (1% to 1.3%) and combined low non-saturable losses (<0.2%) and fast recovery times. Furthermore, we measured a significantly higher F_2 parameter, which resulted in increased reflectivity rollover fluence F_0 and enhanced damage thresholds: our best SESAMs could withstand fluences of up to 100 mJ/cm^2 before damage occurred. Strain compensation guaranteed a low surface defect density and, combined with the decreased field intensity enhancement factor, provided a beneficial reduction of the overall losses. In the future, further optimization and increased accuracy in strain-compensation will in principle enable SESAMs with an even larger number of QWs, producing devices with even higher damage thresholds. In principle, these high-damage threshold SESAMs can easily be designed with higher modulation depth for lasers with very short pulse durations, by simply reducing the number of dielectric top layers.

Optics EXPRESS

We are also interested to reproduce such strain-compensated SESAMs with a phosphorus-MBE system. Additionally, the use of deposition machines with higher accuracy and better material homogeneity compared to PECVD for the dielectric top coatings (i.e. ion beam sputtering, IBS) will also be explored. We expect that this new generation of SESAMs will be a key enabler for further peak power scaling of ultrafast solid-state laser oscillators.

Funding

Swiss National Science Foundation (SNSF-project 152967); Swiss Confederation Program Nano-Tera.ch, which was scientifically evaluated by the Swiss National Science Foundation (SNSF); Swiss Innovation Promotion Agency with the CTI contract No. 17137.1 PFNM-NM.

Acknowledgments

The authors acknowledge support of the technology and cleanroom facility FIRST for advanced micro- and nanotechnology and the Electron Microscopy Center EMEZ of ETH Zurich.